scientific reports

Check for updates

OPEN

The impact of obstacle parameters on mid-high frequency noise propagation in comprehensive mining workfaces and safety implications

Gaini Jia[1,2], Ming Yang[2,3]✉, Dongjie Jiang[1]✉, Junjie Guo[1], Maomao Liu[2] & Yunqi Tao[1]

Noise pollution in fully mechanized mining workfaces threatens the occupational health and safety of miners. Obstacles such as mechanical equipment and pipelines in roadways can alter noise propagation patterns, and clarifying this influence is crucial for mine noise control and personal protection. This study established numerical simulation models for medium- and high-frequency noise propagation in fully mechanized mining workfaces using the finite element method and ray acoustics method within the acoustic module. The reliability of the models was validated by comparing the simulation results with field measurement data from test roadways. On this basis, the influence laws of key parameters such as obstacle obstruction rate, shape, number, and spacing on noise propagation were analyzed. The results show that the obstruction rate and shape of obstacles have a weak impact on the attenuation of mid-to-high-frequency noise, and the noise reduction effect is negligible. When the number of obstacles is fixed, a spacing of 1m achieves a significant noise reduction effect on high-frequency noise (sound pressure level change of approximately 20 dB) but has little impact on mid-frequency noise at 2000 Hz. The number of obstacles significantly affects high-frequency noise, and the optimal configuration is related to spacing—under a spacing of 1m, a single obstacle can achieve significant noise reduction (>10 dB); under a spacing of 3m, 1 or 4 obstacles yield the optimal effect (approximately 20 dB), while their impact on mid-frequency noise is negligible. The research results provide a key basis for mine noise control and obstacle configuration optimization, and have practical value for improving the occupational health protection of miners and ensuring the safe production of coal mines.

Keywords Fully mechanized mining face, Obstacles, Noise propagation, Mid-high frequency noise, Numerical simulation

In recent years, with the widespread use of high-power mining machinery and equipment, the noise intensity in coal mine underground workplaces has become extremely high, making them one of the most severely noise-polluted workplaces[1–3]. In China, coal mine fully mechanized mining workfaces have a variety of noise sources, with high noise intensity from individual machines, primarily in the mid-to-high frequency range[4], and a high rate of individual noise exposure exceeding standards in key underground positions[5]. Long-term exposure to high environmental noise levels can easily lead to hearing loss[6,7], affect mental and physical health[8–13], and impact safety behavior[14–16]. Noise pollution has become a coal mine occupational safety and health issue that coexists with other hazards such as dust, high temperatures, and high humidity[17].

Regarding the characteristics and control technologies of coal mine noise, academic circles have conducted a series of studies: Peng et al[18] studied the noise attenuation characteristics of coal mine tunnelling workfaces through actual measurements and theoretical analysis; Xie et al[19] established an acoustic model for straight

[1]School of Resources and Safety Engineering, Henan University of Engineering, No. 1 Wenchang North Road, Longhu, Xinzheng, Zhengzhou 451191, Henan, China. [2]School of Safety Science and Engineering, Henan Polytechnic University, Jiaozuo 454003, Henan, China. [3]Zhengzhou Institute for Advanced Research of Henan Polytechnic University, Zhengzhou 451464, China. ✉email: yming@hpu.edu.cn; 81083584@qq.com

tunnels based on the surface integral method, investigating the effects of wall absorption coefficients and cross-sectional dimensions on tunnel sound fields; Yang et al[20] used the finite element method to simulate the impact of changes in tunnel cross-sectional dimensions on noise attenuation processes within coal mine tunnelling tunnels; Zhai et al[21] analyzed the attenuation characteristics of local ventilation fan noise in straight tunnels under different wall roughness conditions using a scaled model; Jing et al[22] used the finite element method to study the acoustic field characteristics of a coal cutter in a comprehensive mining face when it was activated at different positions; Yang et al[23] simulated and analyzed the impact of tunnel layout in a comprehensive mining face system on acoustic field characteristics.

Although existing research has made progress in areas such as noise attenuation characteristics and the influence of tunnel structural parameters, it has primarily focused on the harm caused by noise to miners' health and the propagation patterns of noise within tunnels, with insufficient attention given to the impact of obstacles such as mechanical equipment and pipelines commonly found in the complex environment of fully mechanized mining faces. Given that experimental measurements struggle to maintain consistency across multiple measurements and the limited acoustic parameters that can be collected in a given space, numerical simulation techniques offer a flexible means of controlling various influencing factors, providing an effective tool for systematically investigating the mechanisms by which obstacles affect noise propagation. Based on this, this study takes a comprehensive mechanized mining face at a mine in Pingdingshan City, Henan Province, as the research object. Using COMSOL numerical simulation software, the study simulates and analyses the impact of obstacles on noise propagation attenuation within mine tunnels, aiming to provide theoretical basis and technical guidance for systematic noise control and individual occupational health and safety protection in comprehensive mechanized mining faces.

Establishment and validation of noise propagation models in tunnels

Spectral analysis and sound pressure level testing of coal mining machines and noise levels in mine tunnels

The specific standards referenced for on-site noise measurement include: 'Measurement of Physical Factors in the Workplace - Part 8: Noise' (GBZ/T189.8—2007), 'Electroacoustic Sound Calibrators' (GB/T15173-2010), and 'Noise Measurement Point Method for Rock Tunnel Excavation Machinery and Equipment in Coal Mines' (MT/T515-1995).

When conducting on-site measurements of noise levels during coal mining machine operations using an explosion-proof YSD130 sound level meter, select a fast-sampling frequency (FAST, sampling every 125 milliseconds) based on the noise characteristics to capture instantaneous noise levels. Additionally, the A-weighted frequency (dB) is selected to align with human auditory perception, combined with the fast (F) time weighing to reflect noise changes. The equivalent continuous A-weighted sound level (L_{eq}) is used as the indicator for assessing the noise level in the working environment, with its calculation formula as shown in (1).

$$L_{eq} = 10\ \lg\left(\frac{1}{T}\int_0^T 10^{0.1\cdot L_A}dt\right) \tag{1}$$

In the formula: L_{eq} is the equivalent continuous A-weighted sound level, dB; T is the measurement duration, s; L_A is the instantaneous A-weighted sound level at time t, dB.

Select five consecutive working days to measure the noise levels in the working environment of the comprehensive mining face. Set up noise sampling measurement points near the coal mining machine. Measurements are taken randomly once per hour, with each measurement lasting 20 minutes, and eight measurements are taken per working day. During the testing process, data is stored using the data recording function of the sound level meter. After testing, the data is further processed and analyzed using professional software to ensure the accuracy and reliability of the measurement results.

Coal mining machine spectral signal processing involves converting time-domain signals to the frequency domain through Fourier transform (FT), a process that reveals the characteristics of the signal in the frequency domain. Time-domain signals are decomposed into a linear combination of sine waves through Fourier transform, while inverse Fourier transform (IFT) converts the frequency domain back to the time domain. For non-periodic audio signals defined on the entire real number domain, when the periodic signal's Fourier series approaches infinity, it can globally represent the non-periodic signal. The programs in the MATLAB Acoustics Toolbox can perform this transformation, enabling a detailed analysis of the spectral characteristics of coal mining machine audio signals. The spectral diagram of the coal mining machine during operation is shown in Fig 1.

The noise spectrum analysis of the coal mining machine presented in Fig 1 clearly indicates that the majority of noise energy is concentrated within 4000 Hz. Previous research literature[21,24] categorizes noise into low-frequency and mid-frequency (125–160 Hz), mid-high-frequency (200–2500 Hz), and high-frequency (2500-8000 Hz); low-frequency and mid-frequency (frequencies below 500 Hz), mid-frequency (frequencies between 500–2000 Hz), and high-frequency (frequencies above 2000 Hz). Based on the previous classification of low-frequency/mid-frequency, mid-frequency, and high-frequency noise, in the fully mechanized mining face, the noise environment to which workers are exposed includes low-frequency/mid-frequency, mid-frequency, and high-frequency noise, but mid-high-frequency noise is predominant. The mid-frequency range primarily concentrates around 2000 Hz, while the high-frequency range primarily concentrates around 4000 Hz. The statistical distribution of energy across high- and medium-frequency bands in coal mining machines is shown in Table 1.

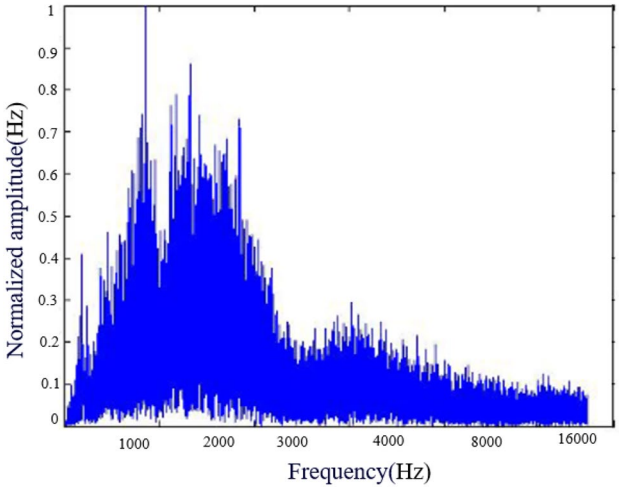

Fig. 1. Shearer noise spectrum diagram.

(1 kHz–8 kHz) 1/3-octave center frequency	L_p(dB)	Relative energy $E \propto 10^{0.1L_p}$	Interval energy proportion
1000	102	$10^{10.2} \approx 1.58 \times 10^{10}$	8.2%
1250	104	$10^{10.4} \approx 1.58 \times 10^{10}$	13.0%
1600	106	$10^{10.6} \approx 1.58 \times 10^{10}$	20.6%
2000	108	$10^{10.8} \approx 1.58 \times 10^{10}$	16.3%
2500	107	$10^{10.7} \approx 1.58 \times 10^{10}$	13.0%
3150	106	$10^{10.6} \approx 1.58 \times 10^{10}$	10.3%
4000	105	$10^{10.5} \approx 1.58 \times 10^{10}$	8.2%
5000	101	$10^{10.1} \approx 1.58 \times 10^{10}$	3.3%
6300	99	$10^{9.9} \approx 1.58 \times 10^{10}$	2.1%
8000	98	$10^{9.8} \approx 1.58 \times 10^{10}$	1.6%
Total (1 kHz-8 kHz)	-	3.85×10^{11}	100%
2 kHz–4 kHz Subtotal	-	1.85×10^{11}	62%

Table1. Statistical table of energy distribution in the mid-to-high frequency range of coal cutters.

Noise exposure calculation

Based on the field measurement data from Section "Spectral analysis and sound pressure level testing of coal mining machines and noise levels in mine tunnels" (L_{eq} of coal mining machine operation noise, 8-hour daily work shift for workers), and in accordance with the requirements of the "Industrial Enterprise Design Hygiene Standards" (GBZ 1–2024)[25], the equivalent continuous A-weighted sound level method was employed to calculate worker noise exposure. The formula adopts Equation (2) with the addition of time-weighting logic[26]:

$$L_{eq} = 80 + 10\lg\frac{\sum_{n} 10^{\frac{(n-1)}{2}} \cdot T_n}{480}(\mathrm{dB}) \tag{2}$$

In the formula, n denotes the segment number of the central sound level, where n = 1 to 8 as shown in Table 2. Tn represents the accumulated exposure time in minutes for the central sound level of segment n within a workday. 480 corresponds to the minute value converted from 8 hours.

Testing revealed that the cumulative noise exposure times during working days at the fully mechanized mining face were as follows: 90 dB for 4 hours, 76 dB for 2 hours, and 100 dB for 2 hours. According to Table 1, the 90 dB noise falls within the central noise level segment with segment number n=3, while the 100 dB noise corresponds to segment number n=5. The 76 dB noise can be disregarded. Therefore, calculation using Equation (3) yields:

$$Leq = 80\mathrm{dB} + 10\lg\frac{10^{(3-1)/2} \times 240 + 10^{(5-1)/2} \times 120}{480}\mathrm{dB} = 94.8\mathrm{dB} \tag{3}$$

Section Number	1	2	3	4	5	6	7	8
Center Sound Level(L_i)/dB	80	85	90	95	100	105	110	115
Exposure time(T_n)/min	T_1	T_2	T_3	T_4	T_5	T_6	T_7	T_8

Table 2. Center Sound Level and Exposure Time for Each Segment.

Calculations indicate that workers in fully mechanized mining faces experience 8-hour noise exposure levels exceeding the 85 dB occupational exposure limit specified in GBZ 2.2–2007.2, indicating a significant risk of hearing damage[8]. This finding provides quantitative evidence supporting the practical significance of subsequent analyses on the noise reduction effectiveness of barriers.

Mathematical equations and model solutions for noise propagation in tunnels

Finite element discretization of sound waves

In the tunnel, the air medium is uniform, and viscosity and heat conduction conditions can be ignored. The three-dimensional wave equation under small amplitude wave conditions is obtained from the continuity equation, state equation, and motion equation. To simplify the problem, the following assumptions are made:

(1) Air is an ideal fluid with no viscosity, so there is no energy loss during the transmission of sound waves.

(2) In the absence of sound disturbances, air is macroscopically stationery and uniform, with constant static pressure and static density.

(3) During the propagation of sound waves, the processes of compression and rarefaction of air are adiabatic, with no energy exchange.

The three-dimensional wave equation for sound waves is:

$$(\frac{\partial^2 p}{\partial x^2}+\frac{\partial^2 p}{\partial y^2}+\frac{\partial^2 p}{\partial z^2})-\frac{1}{c^2}\frac{\partial^2 p}{\partial t^2}=0 \tag{4}$$

where p is the sound pressure, Pa; c is the sound velocity, m/s; t is the time, s; and x, y, z are the spatial coordinates.

The basic idea of solving the wave equation using the finite element method is to transform the variational problem of the entire region into an extremum problem of discrete elements[27]. The object of study is divided into continuous, non-intersecting elements, and specific points on the element boundaries are selected as nodes to construct element approximation functions. Then, the sound pressure on the element can be expressed as:

$$P=[N_a]^T[P_e] \tag{5}$$

In the formula, N_a is a shape function, commonly used polynomial representation, P_e sound pressure vector. The finite element discrete equation of acoustic wave is:

$$[M_e^P][\ddot{P}_e]+[K_e^P][\dot{P}_e]+\rho_0[R_e]^T[\ddot{u}_e]=[0] \tag{6}$$

where $[M_e^P]$ represents the fluid quality matrix, $[K_e^P]$ is the fluid attenuation matrix, $[R_e]^T$ is the contact coupling mass matrix, ρ_0 is the density, and $[\ddot{u}_e]$ is the nodal displacement vector.

As can be seen from equation (6), after determining the shape function of the node function constructed on the unit, the denser the number of units divided the more accurate the results obtained. Based on the wavelength of the acoustic wave, the grid can be divided to consider the effect of its volatility on the acoustic field, a wavelength ($\lambda=c/f$, where c is the speed of sound, f for the acoustic frequency) divided into the number of grids N increased from 1 to 7, to monitor the same point of the change in SPL under different conditions, as shown in Fig. 2.

As can be seen from Fig. 2, with the increase of N, the difference in the calculation results of the SPL of the monitoring points gradually narrows. When $N \geq 4$, the calculation results of the SPL under the conditions of different wavelengths tend to be the same, which leads to the maximum value of the mesh size being set as $\lambda/5=c/f/5$. However, with the increase of the research frequency, the mesh to be divided into the three-dimensional research object is growing as a power function. When analyzing high-frequency noise, the use of ray acoustics can obtain a more accurate solution and can effectively improve computational efficiency.

Solution of ray acoustic simulation model

The ray acoustic method ignores the fluctuation of sound waves and regards sound waves as rays. The propagation state of each ray is described by the process function equation and the intensity equation.

$$(\nabla\varphi)^2=n^2(x,y,z) \tag{7}$$

$$\nabla^2\varphi+\frac{2}{A}\nabla A\cdot\nabla\varphi=0 \tag{8}$$

$\nabla\varphi$ is an eikonal function, φ is the length dimension, n is the direction of acoustic energy propagation, A is the acoustic amplitude, and the equation is an eikonal function equation.

The accuracy of the calculation results of the ray acoustic method depends on the number of rays ray[28,29], the size of which is proportional to the volume V of the study object[30]. In order to explore the relationship between

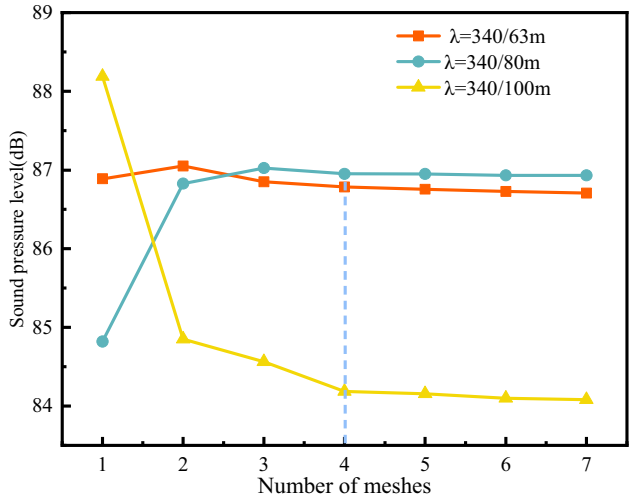

Fig. 2. Convergence check curve of sound pressure level at different wavelengths.

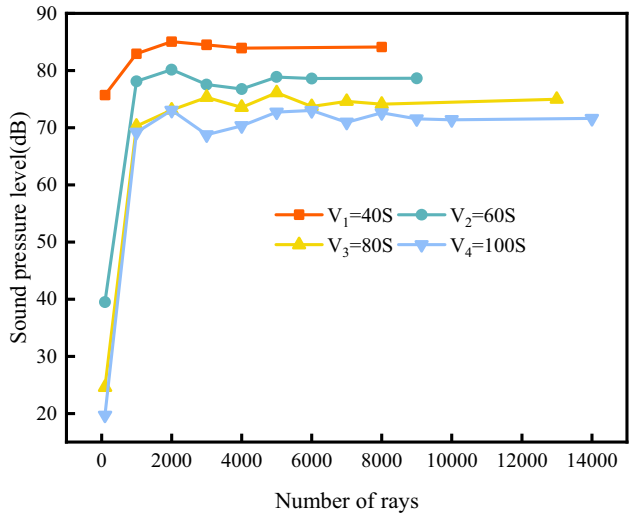

Fig. 3. Convergence check curve of sound pressure level under different volume conditions.

ray and V, the sound field of a rectangular tunnel with a cross-sectional area of S (4.8 m*3.2 m) and volumes of 40S, 60S, 80S and 100S were calculated, and the monitoring point was 10 m away from the port. The change of SPL under different volume and ray conditions is shown in Fig. 3. It can be seen that in the same volume, the increase of ray, the calculation result tends to be stable, and the numerical relationship between ray and volume is ray $N_{ray} \geq 100V$.

Considering the limitations of the finite element method in high-frequency simulation and its applicability in the mid-frequency range, combined with the characteristics of coal mining machine noise, which is mainly in the mid-to-high frequency range, this paper uses the finite element method to simulate mid-to-high frequency noise and combines the geometric sound ray method to treat high-frequency noise in order to effectively analyze the noise propagation characteristics of different frequency ranges.

Verification of mathematical model for noise propagation in tunnels

The Pressure Acoustics and Ray Acoustics interfaces in COMSOL software can simulate acoustic effects, including scattering and diffraction. The Pressure Acoustics interface supports finite element analysis in both the time domain (based on the scalar wave equation) and the frequency domain (based on the Helmholtz equation); the Ray Acoustics interface is used to calculate acoustic ray characteristics. This study focuses on noise attenuation in coal mine tunnels, involving scattering and reflection phenomena, and examines sound wave trajectories and intensity. Based on this, the pressure acoustics and ray acoustics interfaces in COMSOL were used for simulation. The model is based on a rectangular cross-section of 4.8 m × 3.2 m for a fully mechanized mining face, with the physical model shown in Fig 4.

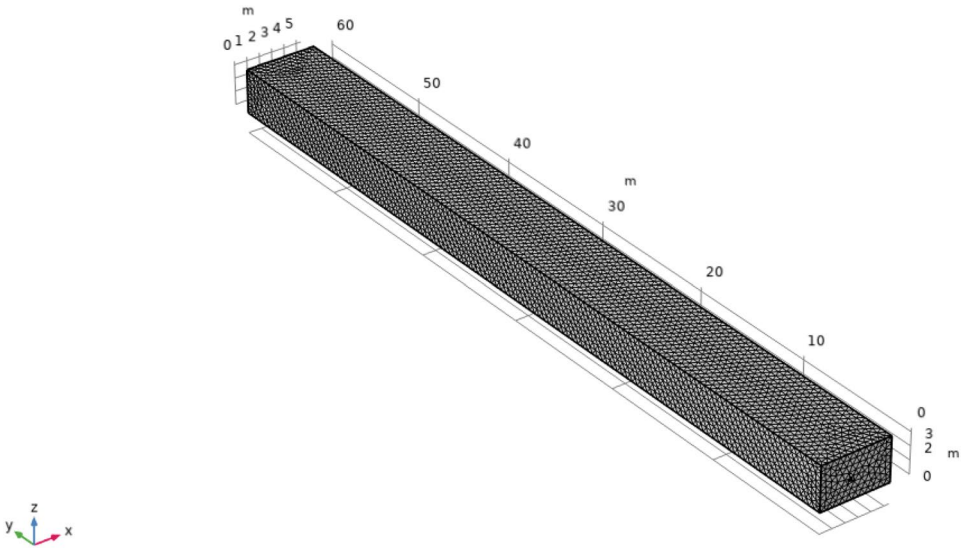

Fig. 4. Physical model and meshing.

The roof and floor strata of the mine tunnel are composed of sandpaper mudstone and fine-grained sandstone, both with sound absorption coefficients of 0.2. The sound absorption coefficients of the coal walls on both sides are 0.3. Given the characteristics of the longwall mining method, the tunnel model is set to infinite length to avoid the influence of end reflections, and the model impedance is set to 1. The mine environmental conditions are: temperature 30 °C, relative humidity 60%, and atmospheric pressure 100 kPa. The most significant noise source in the fully mechanized mining face system is the coal cutter. The noise characteristics of the coal cutter are used as the input sound source for this model.

Numerical simulation primarily explores the noise propagation characteristics of the coal mining process. Noise source parameters are set to match actual measurements taken at the site. The noise generated by coal mining machines can be categorized into exhaust noise, impact noise, rotational noise, and drill rod noise. In reality, these are a combination of quadrupole sources, dipole sources, and monopole sources. In numerical simulations, they are uniformly set as monopole sources[31,32]. The sound power level of the coal mining machine is 110 dB, corresponding to a sound power of 0.1 W.

$$L_W = \lg \frac{W}{W_0}(\mathrm{B}) = 10 \lg \frac{W}{W_0}(\mathrm{dB}) \tag{9}$$

Where, L_W is the sound power level of the source, W; W_0 is the reference sound power, taking the value of 10^{-12} W.

Within the human auditory frequency range of 20 Hz to 20 kHz, due to the limited resolution of adjacent frequencies, a logarithmic frequency band division strategy is adopted to achieve non-uniform frequency band distribution, ensuring high resolution in the low and mid-frequency bands and low resolution in the high-frequency bands. Using the center frequencies of each band as representatives simplifies spectral characteristic analysis. Typical octave center frequencies include 31.5 Hz, 63 Hz, 125 Hz, 250 Hz, 500 Hz, 1 kHz, 2 kHz, 4 kHz, 8 kHz, 16 kHz, etc.

Based on the spectral characteristics of the coal mining machine described in Section "Spectral analysis and sound pressure level testing of coal mining machines and noise levels in mine tunnels", a frequency analysis method using octave bands was employed. The specific frequencies studied included 31.5 Hz, 63 Hz, 125 Hz, 250 Hz, 500 Hz, 1 kHz, 2 kHz, and 4 kHz. Through simulation, noise attenuation contour plots were obtained at different frequencies, as shown in Fig 5.

In order to better reflect the attenuation characteristics of different noise frequencies propagating in the tunnel, the sound pressure levels at each monitoring point were plotted as sound pressure level attenuation curves, as shown in Fig 6.

Fig 6 shows that the noise sound pressure level decreases with increasing distance, consistent with the $y = a \ln x + b$ model ($R^2 > 0.7$). High-frequency noise decays more rapidly, with the absolute value of coefficient a increasing with frequency. By comparing numerical simulations and measured results for 2000 Hz and 4000 Hz noise, the applicability of the selected mathematical model for studying acoustic problems in confined spaces was verified. The measured values and numerical simulation results of sound pressure level decay at a height of 1.5 m above the center of the fully mechanized mining tunnel are shown in Fig 7.

Fig 7 shows that both measured and simulated data indicate that noise sound pressure levels decrease with increasing distance from the sound source. At a distance of 25 m from the sound source, the sound pressure level still exceeds the contact limit specified in the Coal Mine Safety Regulations (85 dB), indicating that the working environment for miners is poor. Sadeghi et al[33] found through a literature review on occupational safety and health in the mining industry that there is little monitoring of noise levels in the working spaces where miners

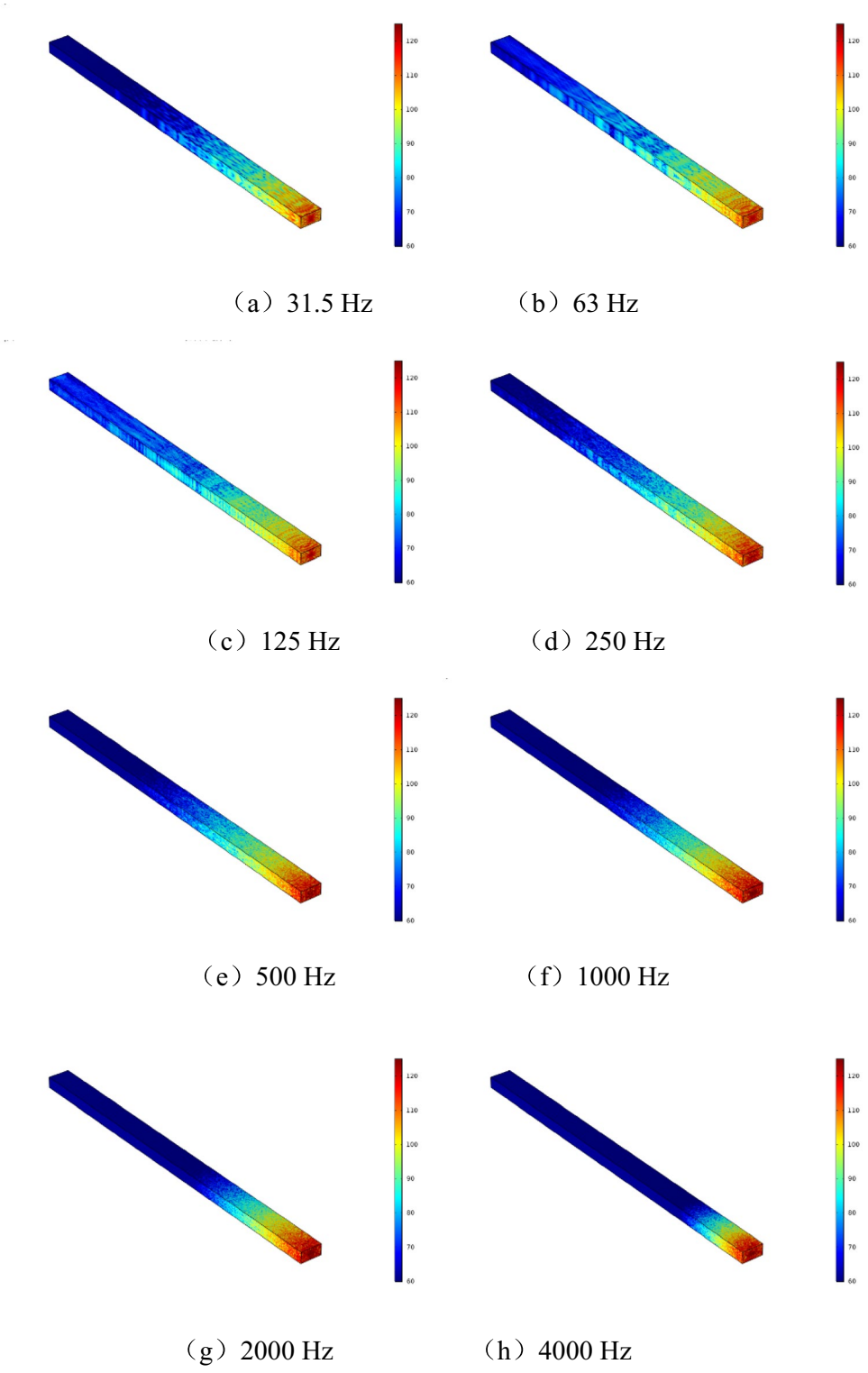

Fig. 5. Sound pressure level nephogram of different frequency noise (unit:dB).

are exposed. Prolonged exposure to high-noise environments increases the risk of hearing loss among miners. Additionally, the measured and numerically simulated sound pressure level variation patterns are consistent, validating the applicability of the finite element method and geometric sound ray method in simulating sound fields in confined spaces.

Although the simulation and actual measurements of noise attenuation in the tunnel show consistent trends, there are systematic deviations: errors in the mid-frequency range (<2000 Hz) are mainly due to the non-uniform distribution of the sound absorption coefficient of the tunnel walls (actual measurements α=0.2~0.5, model fixed

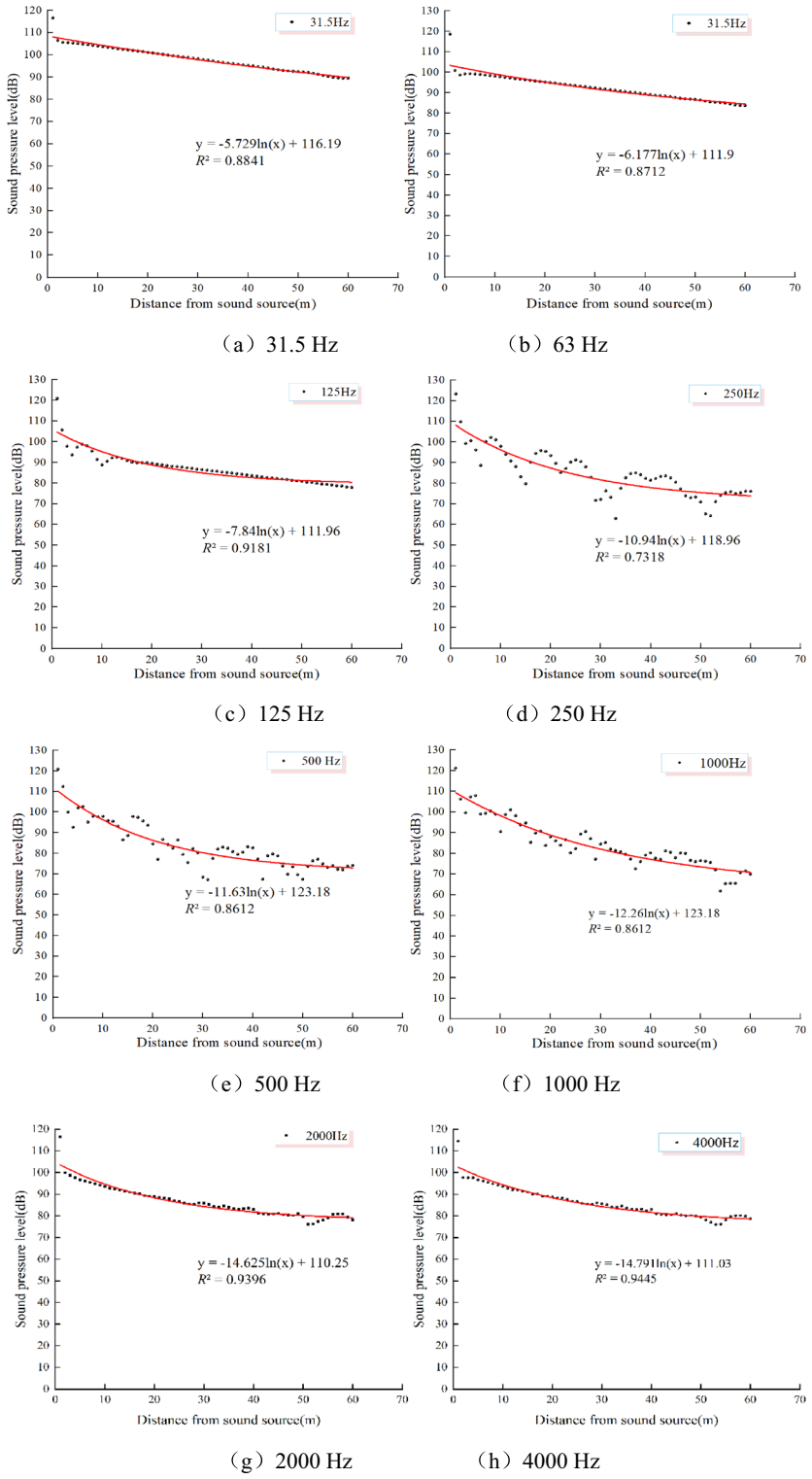

Fig.6. Fitting curve of sound pressure level of different frequency noise with distance attenuation.

at 0.2); errors in the high-frequency range (>2000 Hz) are related to the simplification of the modelling of surface roughness scattering effects (measured roughness R_a = 5 cm results in scattering attenuation at 4000 Hz being higher than the model prediction). Additionally, differences in signal processing introduce errors: measured data uses 1/3 octave band smoothing (Δf = 11.7 Hz), while the model outputs a continuous frequency domain solution, resulting in ±2 dB system deviations at high-frequency peaks.

Given that actual underground measurements interfere with production and the collection of acoustic parameters is limited, this study adopts numerical simulation to comprehensively assess the obstruction effect of

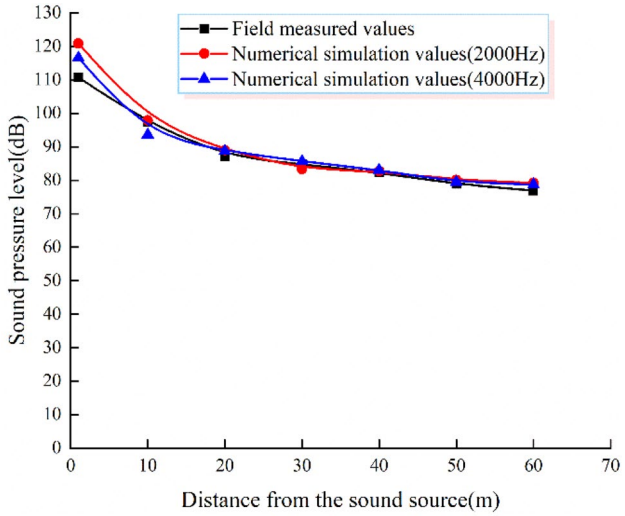

Fig.7. Attenuation curve of sound pressure level at different distances from sound source.

obstacles such as hydraulic supports and pipelines on noise propagation, ultimately providing a feasible solution for predicting sound fields in confined spaces.

Numerical simulation and result analysis of the influence of obstacles on the sound field distribution in the roadway

Obstacle Description

The "obstacles" referred to in this study are natural physical obstacles existing in the fully mechanized tunneling face, rather than specially designed noise control materials. They mainly include two categories: one is mining equipment (e.g., roadheader auxiliary components, scraper conveyors, hydraulic supports, etc.), and the other is underground pipelines (e.g., water supply pipelines, gas drainage pipelines, etc.). Their distribution and dimensions are determined based on on-site actual working condition surveys.

Material and structural parameters of obstacles

Main equipment: Adopts Q235 steel, a commonly used material in underground coal mines, with a density of 7850 kg/m^3 and a thickness of 8–12 mm for key components. It has sufficient structural rigidity to adapt to the harsh underground working environment. Underground pipelines: Selected seamless steel pipes with a density of 7850 kg/m^3 and a diameter of 100–150 mm. Each section of the pipeline is 5–8 m long, arranged at an actual on-site spacing of 1.5–2.0 m.

Acoustic-related characteristics

The above obstacles are all rigid solid bodies (steel-based), and their acoustic impact on noise propagation is mainly reflected in reflection and diffraction effects: Sound absorption characteristics: The absorption coefficient of steel in the mid-high frequency band (1000–4000 Hz) is extremely low (only ~0.01–0.03), almost no sound absorption effect is produced, which is consistent with the acoustic characteristics of rigid materials reported in Zheng et al. (2021)[34]. Key influencing factors: The geometric dimensions (e.g., equipment width of 1.2–1.8 m, pipeline diameter of 100–150 mm) and spatial layout (e.g., equipment spacing of 3–5 m, pipeline height from the ground of 0.8–1.2 m) of the obstacles are the core parameters affecting the noise propagation path and attenuation law. Relevant data have been accurately input into the numerical simulation model

Due to variations in the cross-sectional area, shape, spacing, and number of obstacles in fully mechanized mining roadways, this paper examines the effects of obstacle blockage rate, shape, spacing, and number on the acoustic field within the roadway. Maintaining a sound source power of 0.1 W and considering the characteristic of the coal cutter's frequency spectrum being dominated by mid-to-high frequencies, this study uses 2000 Hz and 4000 Hz as examples to investigate the impact of changes in obstacles within the tunnel on noise propagation in a confined space.

Analysis of the impact of obstacle obstruction rates on sound fields

Given the actual situation in comprehensive coal mining workfaces, where there are numerous mechanical devices of varying shapes and uneven distribution, the obstacle blockage rate r is introduced. The obstacle blockage rate r is defined as the ratio of the cross-sectional area of the obstacle to the cross-sectional area of the tunnel. Since the cross-sectional areas of different mechanical equipment vary, to simplify the study, this mechanical equipment are categorized into different r value ranges based on their cross-sectional areas. Combining field survey data and theoretical analysis, the actual cross-sectional areas of different mechanical equipment in the tunnel were obtained, and the r value ranges were determined. The main mechanical equipment considered in this study and their corresponding r value ranges are shown in Table 3. Although the actual conditions in comprehensive coal

Equipment Name	Equipment Model	Equipment dimensions (length* height*width)/mm^3	The range of values of *r*
Crushing machine	PCM500	2540*1930*1730	≤30%
Shearer	KBSGZY1000/6/1.1	4640*1245*1830	≤20%
Coal mining machine	MG500/1180-WD	3059*1445*1467	
Emulsion pumps	BRW400/31.5	3000*1200*1300	≤10%
Shearer and transporter switches	QJZ700/3300-8	2390*940*1020	
Transfer machine and crusher switch	QJZ630/1140-4	1452*590*725	≤5%
Feeder switch	KBZ400	380*500*700	

Table. 3. Main equipment size parameters.

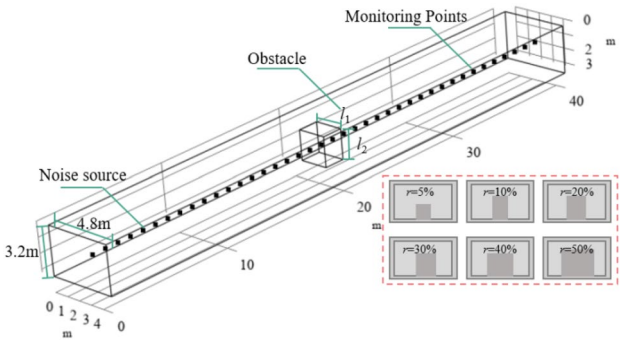

Fig. 8. Schematic diagram of different *r* geometries.

mining workfaces are complex and variable, we have reasonably simplified the research problem by introducing the obstacle blockage rate *r*, addressing the differences in the cross-sectional areas of mechanical equipment, and combining field survey data with theoretical analysis.

During simulation, the values of *r* were set to 5%, 10%, 20%, 30%, 40%, and 50%, with 40% and 50% used as controls. The geometric schematic diagram of the simulation is shown in Fig 8, with the cross-sectional area of the tunnel being 15.36 m^2 (3.2 m × 4.8 m). the sound source is located 8 m along the tunnel's central axis, the obstacle has a square cross-section and is placed at the center of the ground surface, 20 m along the x-axis, with a length equal to the average horizontal length of mechanical equipment (2 m). Monitoring points are set every 1 m along the tunnel's central axis to collect data required for extracting the sound pressure level distribution curve of the tunnel's sound field.

Fig 9 shows the noise field diagrams for frequencies of 2000 Hz and 4000 Hz in a comprehensive mining tunnel under different obstacle blockage rates. As can be seen from the figure, at different frequencies, as the obstruction rate increases, the attenuation of the sound pressure level in the sound field behind the obstacle increases; at the front of the obstacle, the noise field at a frequency of 2000 Hz exhibits standing wave phenomena, which become more pronounced as the obstruction rate increases; high-frequency noise in the sound field in front of the obstacle is less affected by changes in the obstruction rate.

In order to more clearly demonstrate the impact of changes in obstacle obstruction rates on changes in the sound field within the tunnel, sound pressure level data was extracted from a distance of 5 m from the sound source and used to plot a sound pressure level distribution curve within the comprehensive mining tunnel, as shown in Fig 10.

In Fig 10, as sound waves propagate, their energy decreases, and the sound pressure level decreases with increasing distance from the sound source. The presence of an obstacle causes a significant increase in sound pressure level in front of the obstacle. High-frequency sound waves experience greater attenuation than mid-frequency sound waves during propagation. Additionally, the sound field generated by high-frequency sound waves in the tunnel is more fluctuating and unstable. The sound field in front of the obstacle is insensitive to the presence of the obstacle and shows no significant changes. Fig 10(a) shows the sound field in front of the obstacle. As the obstruction rate r increases, the standing wave phenomenon becomes more pronounced, and the increase in sound pressure level in front of the obstacle also increases with r, but the effect is limited, with noise reduction within a 3 dB range. From Fig 10(b), it can be seen that when the obstruction rate is within 20%, changes in the obstruction rate have little effect on the sound field in the tunnel. The sound field behind the obstacle follows the same propagation pattern as mid-frequency sound, and the overall sound pressure level also decreases with increasing obstruction rate r. However, the noise reduction effect is limited. The difference is that the unstable high-frequency sound field in the tunnel becomes even more unstable as r increases. Therefore, the effect of the obstruction rate on noise attenuation within the tunnel can be neglected.

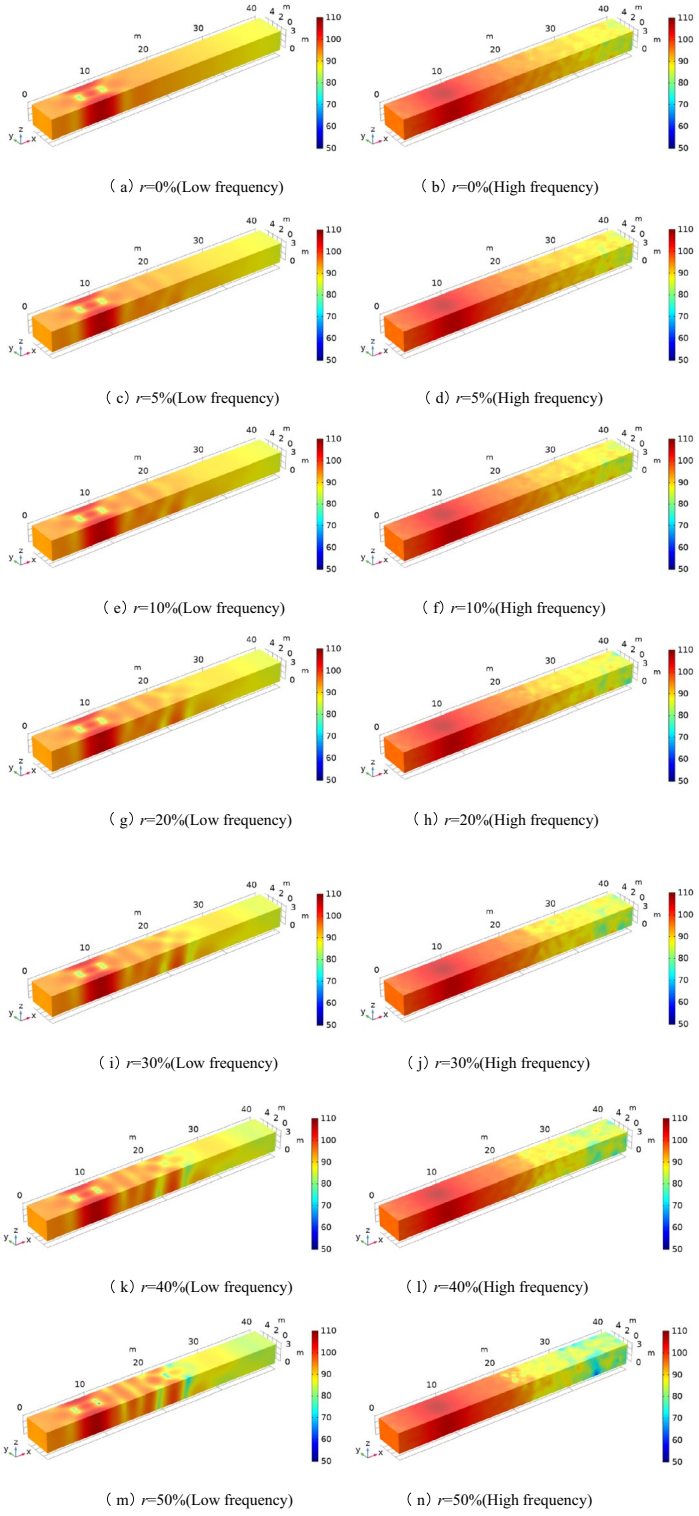

Fig. 9. Sound field distribution of mid -frequency and high-frequency sound in roadway under different *r* conditions(unit: dB).

Analysis of the insfluence of obstacle shape on sound field distribution

Mining tunnel machinery comes in various shapes, with rectangular cross-sections being the primary type. Machinery with rectangular cross-sections typically have a width-to-height ratio ranging from 0.5 to 2. Additionally, the ratio of the cross-sectional area of machinery to the tunnel's cross-sectional area is often around 10%, with the width-to-height ratio ranging from 0.5 to 2. A blockage ratio of r=10% is set. obstacles with rectangular width-to-height ratios of 0.5, 1, 1.5, and 2. The geometric schematic diagram of the simulation

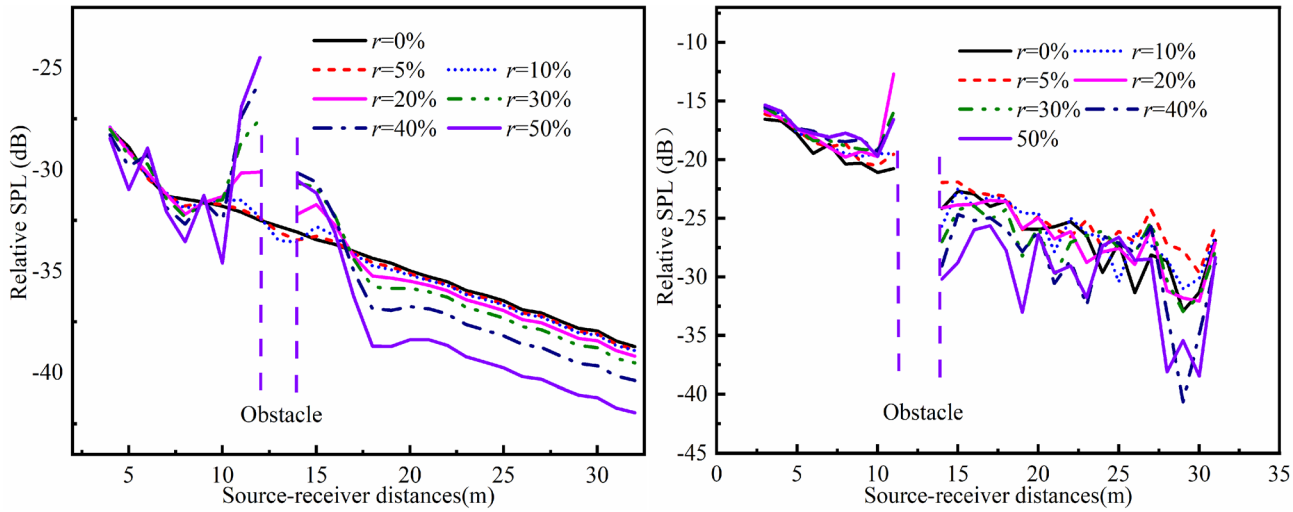

Fig. 10. Sound field distribution curves of mid -frequency and high-frequency sound in roadway under different *r* conditions.

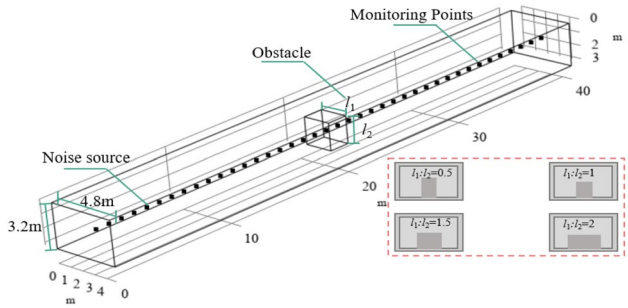

Fig. 11. r=10%, geometric diagram of different obstacle shapes in the roadway.

model is shown in Fig 11. Based on the model calculations, the sound field diagrams of low-frequency, medium-frequency, and high-frequency noise in the tunnel under different obstacle shapes are shown in Fig 12. Additionally, the internal sound pressure level distribution curves are further plotted as shown in Fig 13.

(**a**) Low frequency (**b**) High frequency

As shown in Fig 13, the effects of obstacles of different shapes on the sound field in the tunnel are nearly identical. In Fig 13(a), due to the presence of the obstacle, standing waves are generated in the low-frequency sound field. Before the obstacle, the sound pressure level increases due to sound interference, while in the region above the obstacle, part of the sound energy is absorbed by the obstacle, thereby weakening it; Due to the strong diffraction capability of mid-frequency sound, the sound pressure level behind the obstacle increases. Overall, the obstacle reflects and absorbs part of the sound energy, but the noise reduction effect is within 10 dB and can be ignored. Fig 13(b) shows that taller obstacles can significantly increase the sound pressure level of high-frequency noise at their front end. The sound pressure level at the rear end of the obstacle exhibits an oscillatory decay characteristic along the longitudinal direction. The wider the obstacle, the smaller its height-to-width ratio, and the more pronounced the fluctuations in sound pressure level; Due to the short wavelength and poor diffraction capability of high-frequency noise, it undergoes reflection and scattering when encountering obstacles, resulting in the consumption and attenuation of sound energy. Subsequently, due to the phenomenon of in-phase superposition or phase cancellation among multiple reflected sound waves, the sound pressure level behind the obstacle exhibits significant oscillation. The smaller the width-to-height ratio of the obstacle, the greater the fluctuations in sound pressure levels before and after it. The maximum change in high-frequency noise sound pressure levels is approximately 10 dB. As the distance from the sound source increases, the shape of the obstacle has a negligible effect on the attenuation of low-frequency and mid-frequency noise sound pressure levels. Therefore, the influence of obstacle shape on noise attenuation within the tunnel can be ignored.

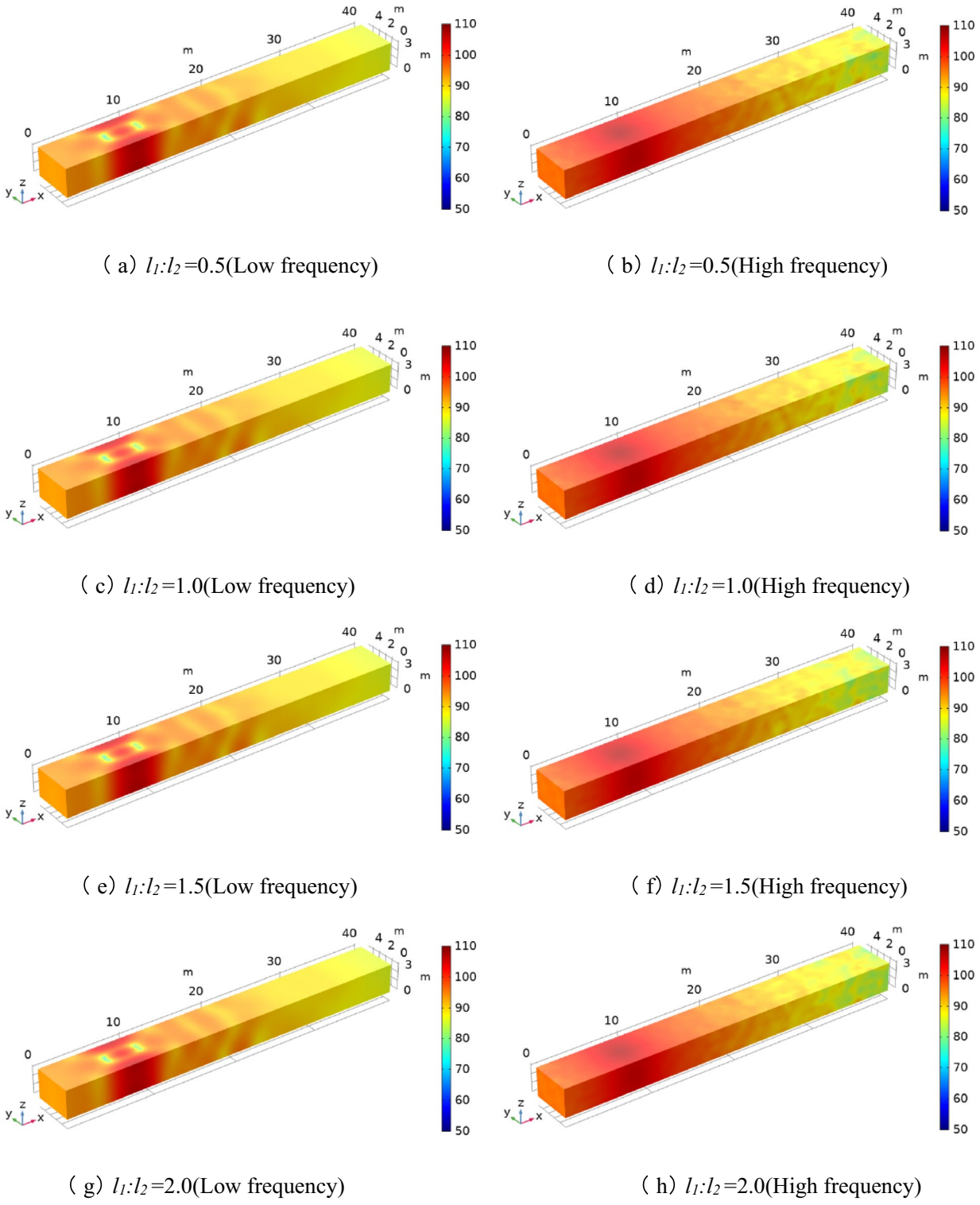

Fig. 12. Cloud distribution of mid -frequency and high-frequency sound in roadway under different obstacle shapes (unit: dB).

Analysis of the influence of obstacle spacing on sound field distribution

As the comprehensive mining system advances forward, auxiliary coal-cutting machinery such as emulsion pumps, coal cutter switches, and crusher switches move forward sequentially. Therefore, the spacing between machinery should not be too tight, as overly loose spacing is also detrimental to the effective utilization of tunnel space. Based on this, it is necessary to investigate machinery spacing that is conducive to sound attenuation. The geometric diagram of obstacle spacing variations in the design tunnel is shown in Fig 14. The obstacle

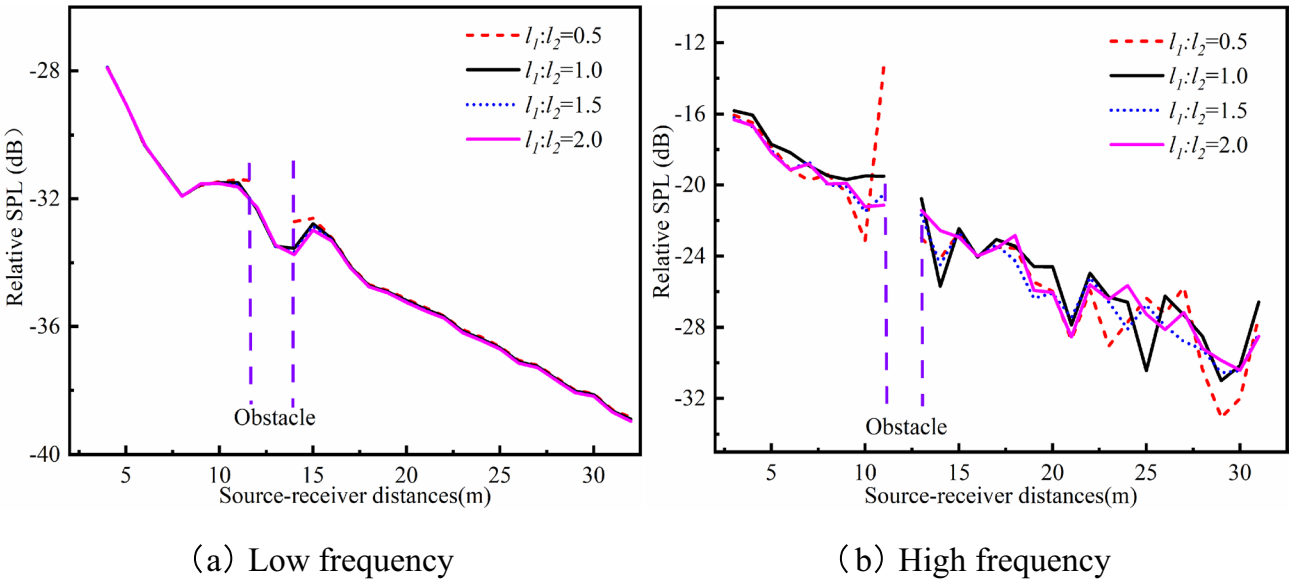

Fig. 13. Sound field distribution curves of mid-frequency and high-frequency sound in roadway under different obstacle shapes.

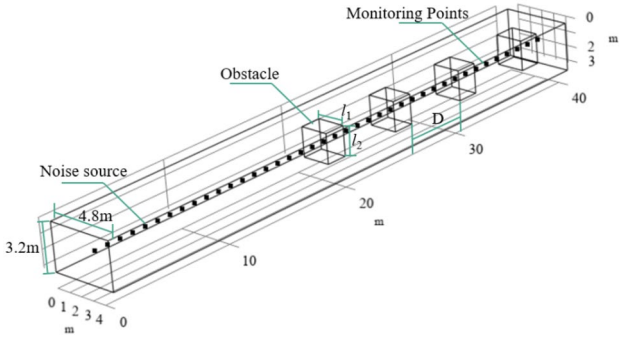

Fig. 14. Geometry of obstacle spacing changes.

blockage rate *r* is 10%, with the first obstacle fixed at the 20 m mark in the tunnel. The spacing D is set to 0.5 m, 1.0 m, 1.5m, 2.0 m, 2.5 m, and 3.0 m. The 0.5 m and 1.0 m settings are considered for some small equipment or components, which have relatively smaller spacing between them; The 1.5 m and 2.0 m settings are designed for medium-sized equipment, such as certain auxiliary devices or components of coal mining machines, where the spacing between them may need to be appropriately increased; For the coal mining machine itself or its critical components, the spacing between them needs to be larger, such as 2.5 m or 3.0 m, to ensure sufficient space for the equipment to move and adjust during operation while preventing safety accidents caused by collisions between devices. Considering the varying number of mechanical devices required for different operations, the sound field curves for low-frequency, medium-frequency, and high-frequency noise in the tunnel were calculated under conditions with 2, 3, and 4 obstacles, as shown in Fig 15, 16, and 17.

As shown in Fig 15, 16, and 17, changes in the spacing between obstacles have no significant effect on the sound pressure level of mid-frequency noise in the tunnel, but they do have a noticeable impact on the sound pressure level of high-frequency noise. Figs 15(a), 16(a), and 17(a) show that the sound field is related to the distance between obstacles. The presence of obstacles causes the sound pressure level of mid-frequency noise in the tunnel to fluctuate. Increasing the distance causes the waveform of the mid-frequency sound pressure level distribution curve to shift backward and downward, but the noise reduction effect is limited, with changes in sound pressure level remaining within 10 dB. Figs 15(b), 16(b), and 17(b) show that when the obstacle spacing is 1.0 m, the changes in sound pressure levels before and after the obstacles are most pronounced, with a noise reduction of approximately 20 dB, and the changes in sound pressure levels are most noticeable on the sound-facing side of the first obstacle.

To visually compare the effect of obstacle spacing on the sound field, cross-sectional diagrams of the sound field in a tunnel containing three obstacles were drawn for low-frequency, mid-frequency, and high-frequency noise under different spacing conditions, as shown in Fig.18.

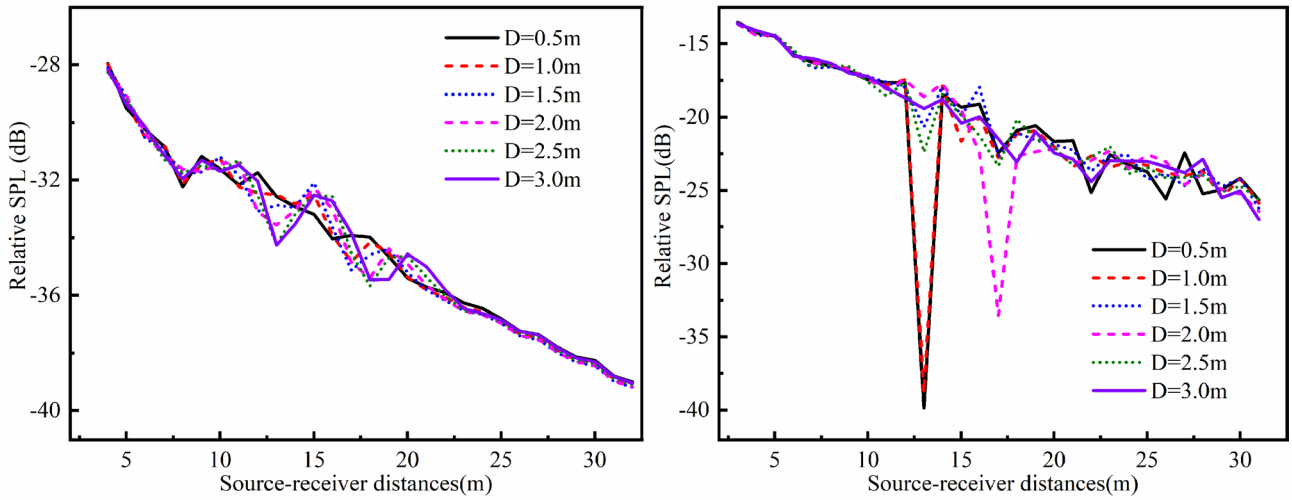

Fig. 15. Sound field distribution curve of mid-frequency and high-frequency sound in a roadway containing two obstacles under different spacing conditions.

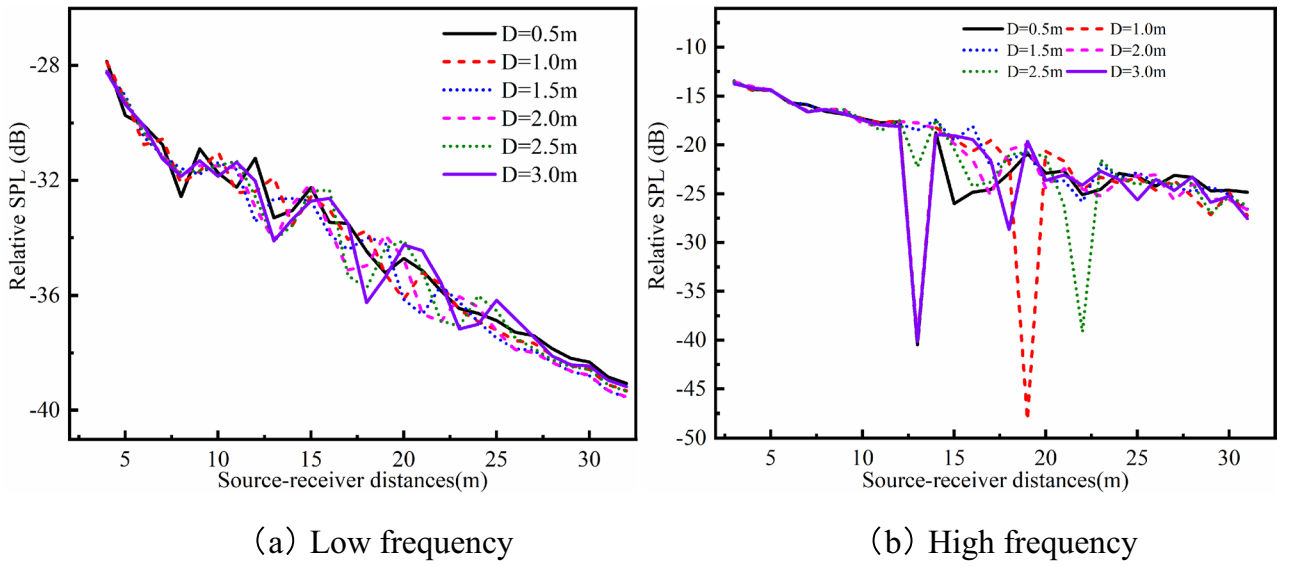

Fig. 16. Sound field distribution curves of mid-frequency and high-frequency sound in a roadway containing three obstacles under different spacing conditions.

Figs 18(a), (c), and (e) show that the sound field of mid-frequency noise in the tunnel is similar, with sound energy primarily concentrated at the front end of the obstacle. Standing waves appear near the obstacle, and as the distance between obstacles increases, the accumulated sound energy between them gradually decreases. This is primarily due to the strong diffraction capability of mid-frequency noise and enhanced interference on the sound-facing surface of the obstacle. As shown in Figs 18(b), (e), and (d), high-frequency noise exhibits similar acoustic field characteristics in the tunnel, with sound energy primarily accumulating on the front surface of the first obstacle. As the distance between obstacles increases, the sound energy at the front of other obstacles gradually weakens, and low-noise regions appear behind the obstacles.

For high-frequency noise (4000 Hz), priority can be given to the obstacle layout with a 1.0 m spacing: a first obstacle is placed at a 1.0 m spacing near the front end of the roadway adjacent to major high-frequency noise sources such as shearers. By virtue of its strong attenuation characteristics for high-frequency noise, efficient blocking is achieved in the initial stage of propagation. The main operating areas for workers are arranged in the low-noise region behind this obstacle, and the spacing of subsequent obstacles is appropriately optimized according to the attenuation law of high-frequency sound energy, thus forming a control system featuring "strong front-end blocking + rear-end regional protection".

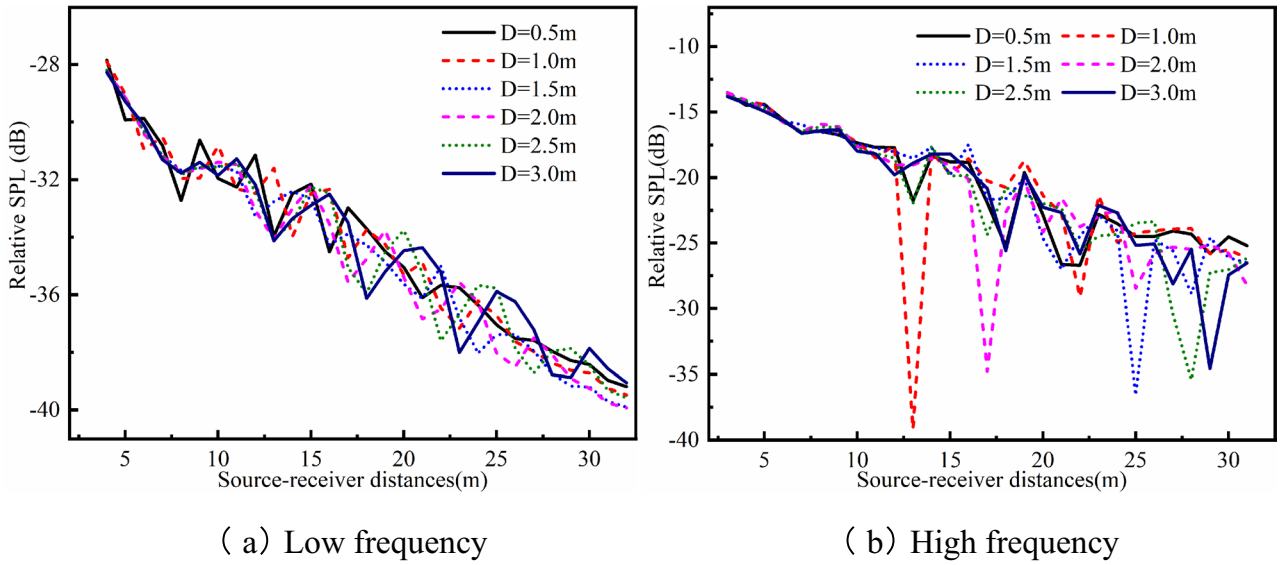

Fig. 17. Sound field distribution curve of mid-frequency and high-frequency sound in a roadway containing four obstacles under different spacing conditions.

For mid-frequency noise represented by 2000 Hz, it is necessary to overcome the limitations of simply adjusting spacing and adopt a dual-pronged approach of 'enhancing the transmission path' and 'controlling the sound source': In terms of transmission pathways, existing obstacles should be upgraded to 'sound-absorbing - sound-insulating composite structures.' For example, on the sound-receiving surface, resonance-based sound-absorbing materials (such as micro-perforated plates) tailored for the 2000 Hz frequency band can be used to absorb sound energy in this frequency range through resonance effects, while sound-insulating layers can weaken sound energy transmitted via diffraction; In terms of sound source control, the focus is on optimizing the structure of the coal cutter head (e.g., adjusting the density of cutting teeth arrangement), selecting low-vibration cutting tooth materials, or installing dampers to suppress vibration radiation in the 2000 Hz frequency band, thereby reducing noise generation at the source.

Future research could further focus on 'multi-frequency band coordinated control': By using numerical simulation to screen for material parameters that optimize resonance absorption at 2000 Hz, combined with tunnel space design to create modular composite obstacles (balancing high-frequency blocking at 4000 Hz and mid-frequency absorption at 2000 Hz), while quantifying the impact weight of cutting parameters on 2000 Hz noise, ultimately forming an integrated system of "source reduction - targeted absorption - high-frequency blocking" integrated system to efficiently reduce mid-to-high-frequency noise dominated by 2000 Hz.

Analysis of the influence of the number of obstacles on the sound field distribution

As shown in Figs.15, 16, and 17, when the spacing is 1 m and 3 m, the changes in sound pressure level of low-frequency, mid-frequency, and high-frequency noise in the tunnel under different obstacle quantities are shown in Figs. 19 and 20.

Analysis of Figs 19 and 20 shows that the number of obstacles in the tunnel has no significant effect on the average level of mid-frequency noise sound pressure in the tunnel but has a significant effect on the level of high-frequency noise sound pressure. For high-frequency noise, when the distance between obstacles is 1 m, changes in the number of obstacles have the same effect on the sound pressure levels before and after the first obstacle, i.e., as the number of obstacles increases, the change in sound pressure levels remains the same, exceeding 10 dB; When the distance between obstacles is 3 m, having only 1 or 4 obstacles significantly affects the sound pressure level before and after the first obstacle, with a change of approximately 20 dB. However, when there are 2 or 3 obstacles, the effect on the sound pressure level before and after the first obstacle is not noticeable.

Further analysis of Figs 19(a) and 20(a) shows that as the number of obstacles increases, the number of waves formed by the sound pressure level distribution curves of low-frequency and mid-frequency noise also increases, exhibiting a positive correlation with the number of waves, and the amplitude of the fluctuations becomes larger. Figs 19(b) and 20(b) show that when the spacing between obstacles is constant, as the number of obstacles increases, the oscillation characteristics of the sound pressure level curve become more pronounced when high-frequency noise propagates through a tunnel with obstacles, and low-noise zones form at the locations of the obstacles.

To clearly compare the effect of the number of obstacles on the sound field in the tunnel, cross-sectional diagrams of the sound field in the tunnel for low-frequency, mid-frequency, and high-frequency noise under different obstacle conditions were drawn at a spacing of 2 m, as shown in Fig.21.

As shown in Fig.21, when the spacing between obstacles is consistent, the sound fields in the tunnel are similar, with sound energy accumulating on the sound-receiving surfaces of the obstacles. As the number of obstacles increases, the accumulation of sound energy in the front regions outside the obstacles gradually decreases. Due

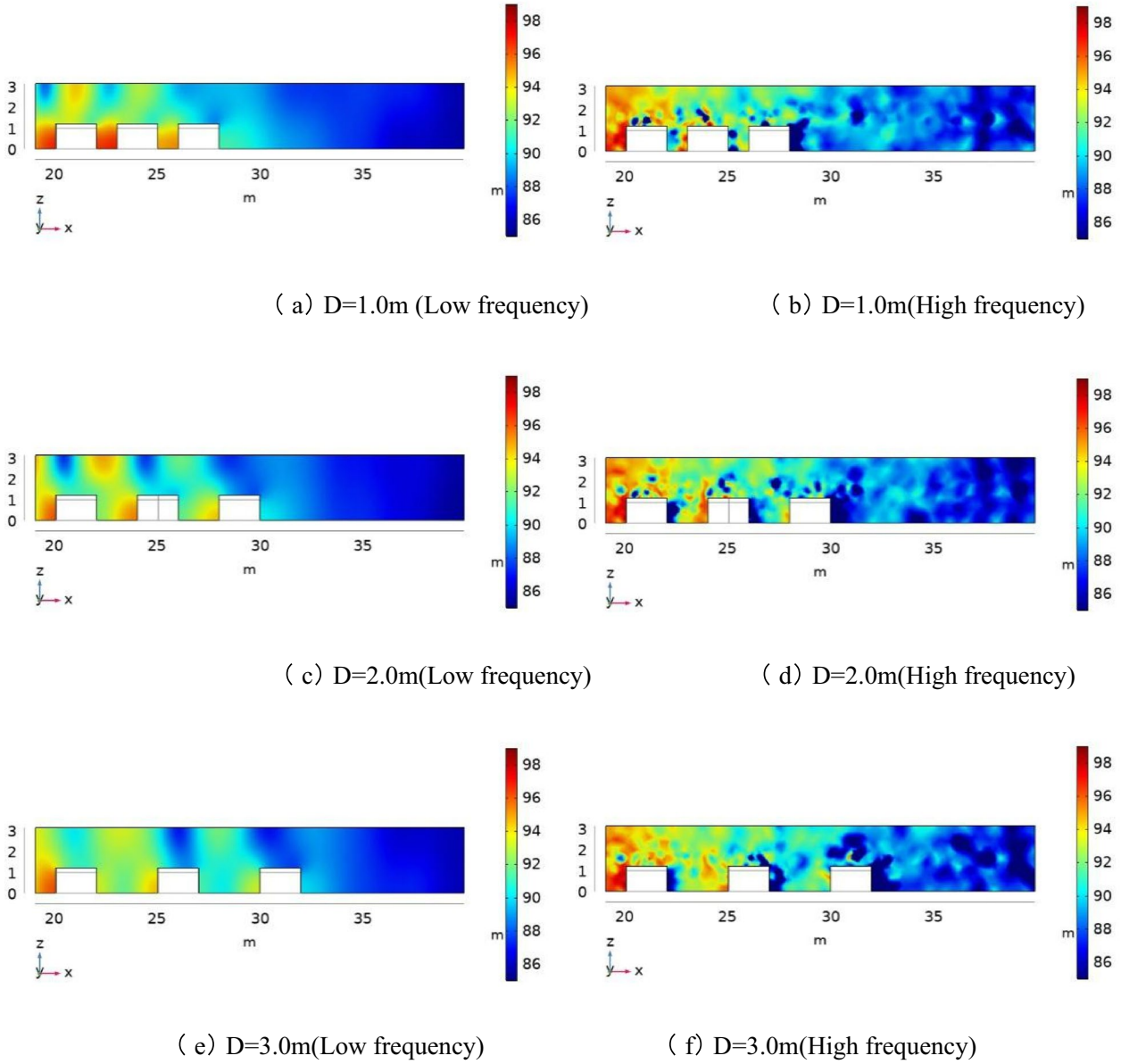

（a）D=1.0m (Low frequency)　（b）D=1.0m(High frequency)

（c）D=2.0m(Low frequency)　（d）D=2.0m(High frequency)

（e）D=3.0m(Low frequency)　（f）D=3.0m(High frequency)

Fig. 18. Cross-sectional view of the sound field distribution of mid-frequency and high-frequency sound in a roadway containing three obstacles under different spacing conditions(unit: dB).

to the large number of obstacles inside the tunnel, the surface area capable of reflecting sound waves increases. Noise attenuation, combined with sound energy absorption at the obstacle surfaces and reflection cancellation, consumes part of the sound energy, thereby reducing the sound pressure level inside the tunnel. Based on simulation patterns, for high-frequency noise, a single obstacle with a spacing of 1 meter can be prioritized for efficient noise reduction, as its effect is equivalent to that of multiple obstacles. When the spacing is 3 meters, either one or four obstacles can achieve significant noise reduction effects without the need to increase the number further. For 2000 Hz mid-frequency noise, changes in the number of obstacles have a negligible effect on noise reduction. Therefore, it is necessary to move beyond the approach of simply adjusting the number of obstacles and instead focus on developing sound-absorbing and sound-insulating composite structures tailored to this frequency band, while optimizing the design of the coal cutter system to address mid-frequency noise reduction challenges from both the propagation path and the sound source end.

Conclusion and future work

This study focuses on the prevention and control of mid-to-high frequency noise (2000Hz mid-frequency, 4000 Hz high-frequency) in fully mechanized mining faces. Through coupled numerical simulations using the finite element method and ray acoustics, combined with field measurements to validate model reliability,

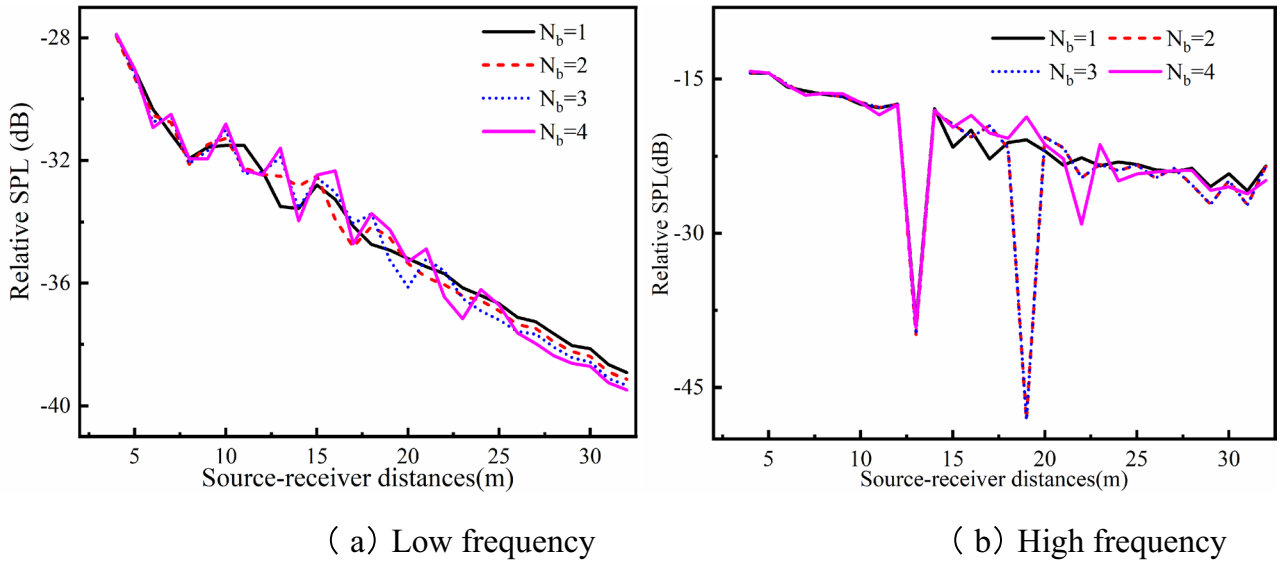

（a）Low frequency　　（b）High frequency

Fig. 19. When the distance is 1 m, the sound field distribution curve of mid-frequency and high-frequency sound in the roadway under different number of obstacles.

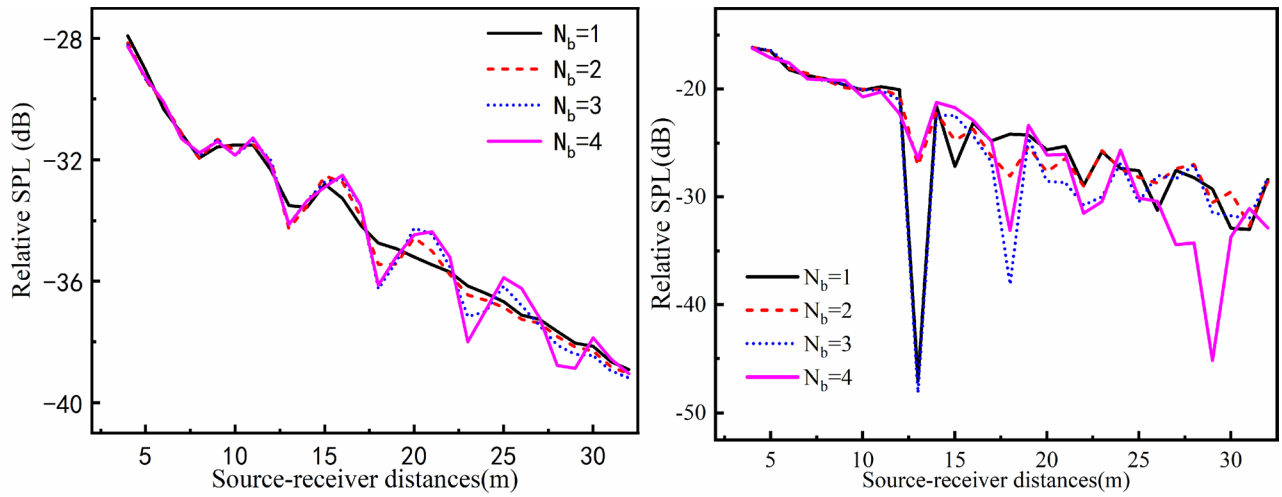

（a）Low frequency　　（b）High frequency

Fig. 20. When the distance is 3 m, the sound field distribution curve of mid-frequency and high-frequency sound in the roadway under different number of obstacles.

it systematically analyzes the impact of key parameters of obstacles within roadways on noise propagation. It identifies engineering-applicable control principles, with primary conclusions as follows:

(1) The obstruction rate (5%–50%) and shape (aspect ratio 0.5–2.0) of obstacles exert negligible influence on mid-to-high-frequency noise attenuation, with noise reduction effects remaining below 3 dB. These parameters can be disregarded in engineering practice and should not be prioritized for noise control optimization.
(2) The regulatory effect of obstacle spacing on noise propagation exhibits significant frequency-specific characteristics: For 4000 Hz high-frequency noise, a 1 m spacing with a fixed number of obstacles achieves approximately 20dB SPL reduction. This attenuation is concentrated on the first obstacle's sound-facing surface near the source, effectively lowering high-frequency noise exposure risks in the work area. For 2000 Hz mid-frequency noise, spacing variations cause only minor fluctuations of ±10dB, yielding no substantial noise reduction.
(3) The number of obstacles significantly impacts high-frequency noise reduction, with optimal configurations matching spacing: At 1 m spacing, a single obstacle achieves >10 dB stable noise reduction, equivalent to

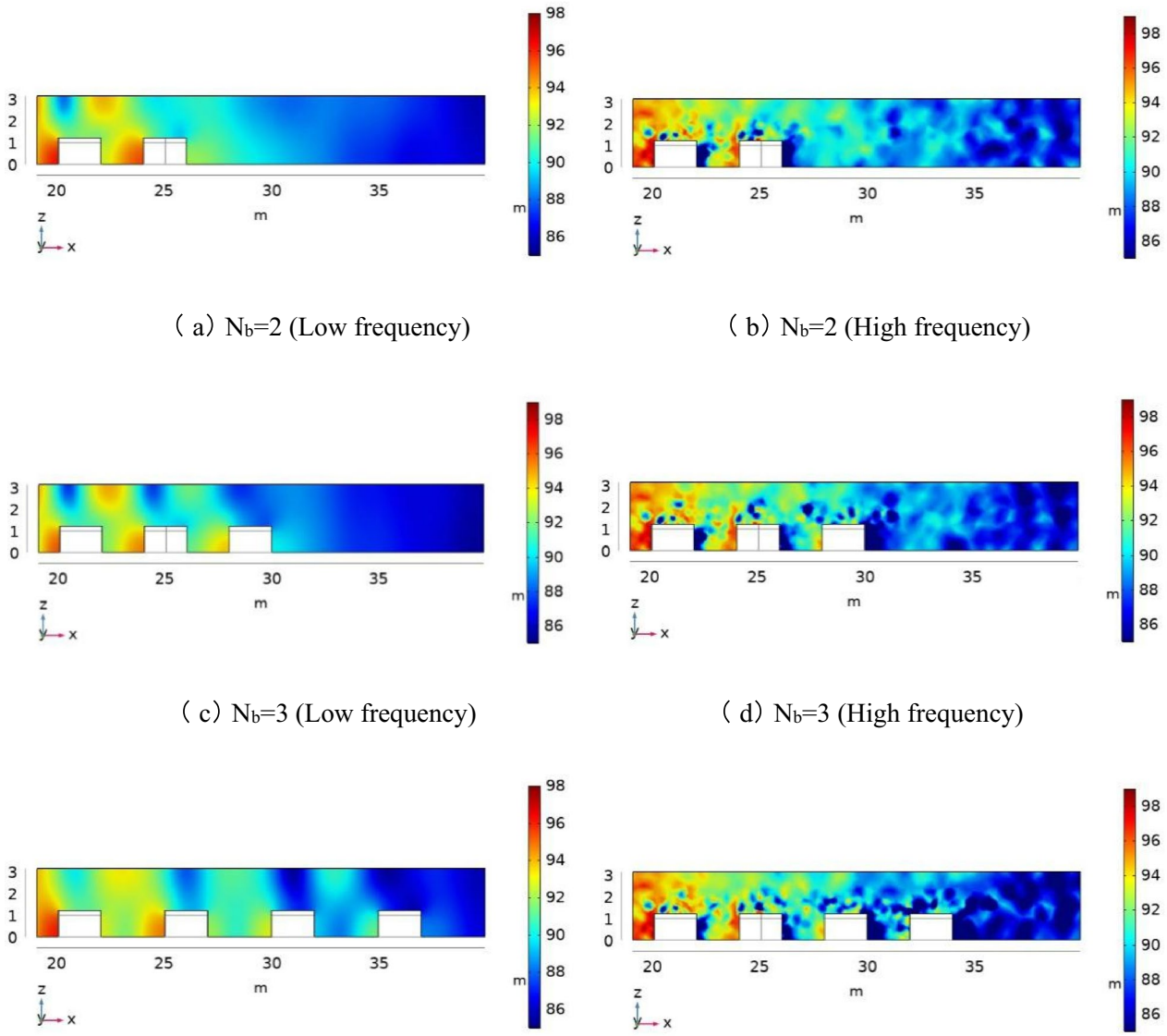

（a）N_b=2 (Low frequency)　（b）N_b=2 (High frequency)

（c）N_b=3 (Low frequency)　（d）N_b=3 (High frequency)

（e）N_b=4 (Low frequency)　（f）N_b=4 (High frequency)

Fig. 21. When the spacing is 2 m, cross-sectional view of sound field distribution of mid-frequency and high-frequency sound in roadway under different obstacle numbers(unit: dB).

multiple obstacles, reducing spatial requirements and costs; At a spacing of 3 m, either 1 or 4 obstacles yield optimal noise reduction (approximately 20 dB). Using 2–3 obstacles weakens attenuation due to sound field superposition, providing precise layout references for different roadway spaces. However, varying the number of obstacles has no significant effect on mid-frequency noise reduction, only affecting the amplitude of sound field fluctuations.

This study has certain limitations: simulations used Q235 steel as a homogeneous material for obstacles, neglecting the impact of surface rust and dust accumulation on acoustic properties of underground equipment; the fixed sound absorption coefficient (0.2–0.3) for roadway walls deviates from the non-uniform distribution caused by variations in coal and rock composition, potentially introducing ±2dB errors between simulated and measured mid-frequency results; The study focused on a single rectangular roadway and a single-source scenario (the coal cutter). The generalizability of these conclusions to scenarios with multiple overlapping sound sources or irregularly shaped roadways requires further validation.

In view of the limitations of the current study, future work can be carried out in the following aspects: First, build a 1:5 scaled mock-up of the fully mechanized mining face, which accurately replicates the obstacle layout, noise source characteristics (including mid-high frequency and low-frequency components), and spatial environment of the actual working face. Conduct experimental measurements of noise propagation under

different obstacle parameters to further verify the reliability of the numerical simulation model and supplement the missing experimental validation of low-frequency noise. Second, combine the scaled mock-up experiment with simulation optimization to explore the influence of obstacle material, spacing, and height on the attenuation effect of multi-frequency noise, providing more precise parameters for engineering application. Third, under the premise of ensuring on-site operation safety, carry out long-term continuous monitoring of noise propagation in the fully mechanized mining face, accumulate practical data to verify the applicability and effectiveness of the proposed obstacle noise reduction scheme in actual production, and provide more reliable technical support for miners' occupational health protection.

Data availability

The data supporting the findings of this study are available from Gaini Jia upon reasonable request. For data access inquiries, please contact Gaini Jia via the QQ email: 849768108@qq.com or 15538059813@163.com.

Received: 15 August 2025; Accepted: 5 December 2025
Published online: 24 December 2025

References

1. Li, J., Qin, Y., Yang, L., Wang, Z. & Guan, C. A simulation experiment study to examine the effects of noise on miners' safety behavior in underground coal mines. *BMC Public Health* **21**(1), 1–12 (2021).
2. Cao, Q., Yu, K., Zhou, L., Wang, L. & Li, C. In-depth research on qualitative simulation of coal miners' group safety behaviors. *Saf. Sci.* **113**, 210–232 (2019).
3. Yang, M., Jia, G., Liu, M. & Quan, X. Scientific knowledge map analysis of coal mine noise research progress in China. *China Saf. Sci. J.* **32**(5), 178–184 (2022).
4. Lei, B. et al. Detection and analysis on the noise source of main equipments in the underground coal mine. *J. North China Inst. Sci. Technol.* **7**(1), 72–75 (2011).
5. Wang, B. et al. Investigation and analysis of harmful degree of underground noise in a coal mine in Shanxi province. *Chin. J. Public Health Eng.* **18**(5), 660–661 (2019).
6. Quick, B. L. et al. An examination of antecedents to coal miners' hearing protection behaviors A test of the theory of planned behavior. *J. Saf. Res.* **39**, 329–338 (2008).
7. Su, Z. et al. The association between occupational noise exposure and hearing loss among petrochemical enterprise workers in Hainan, South China. *Sci. Rep.* https://doi.org/10.1038/s41598-025-90023-1 (2025).
8. Jia, G. et al. Research on occupational health damage in different working places in underground coal mine. *China Saf. Sci. J.* **33**(4), 221–229 (2023).
9. Zare, S. et al. The effect of occupational noise exposure on serum cortisol concentration of night-shift industrial workers: a field study. *Saf. Health Work* **10**(1), 109–113 (2019).
10. Li, B. et al. Quantification study of working fatigue state affected by coal mine noise exposure based on fuzzy comprehensive evaluation. *Saf. Sci.* **146**, 105577 (2022).
11. Liu, C. et al. The effect of the acoustic environment of learning spaces on students' learning efficiency: a review. *J. Build. Eng.* **79**, 107911 (2023).
12. Lercher, P. Environmental noise and health: an integrated research perspective. *Environ. Int.* **22**(1), 117–129 (1996).
13. Rylander, R. Physiological aspects of noise-induced stress and annoyance. *J. Sound Vib.* **277**(3), 471–478 (2004).
14. Fu, W. et al. Experimental study of the influence of coal mine noise on miners. *J. Loss Prev. Process Ind.* **80**, 104926 (2022).
15. Wang, J., Fu, W. & Wang, Y. Study on the effects of different levels of noise on miners' physiological indexes and behavioral abilities. *Mining Saf. Environ. Prot.* **46**(1), 99–103 (2019).
16. Li, J., Cai, Z. J., Liu, Y. H. & Xin, Y. L. Experimental research on the influence of short-term noise exposure on miners' physiology. *Processes* **11**(2), 425 (2023).
17. Yuan, L. Scientific conception of coal mine dust control and occupational safety. *J. China Coal Soc.* **45**(1), 1–7 (2020).
18. Peng, Y. et al. Study about spatial and temporal properties of machine noise source on roadway head of mine. *J. Hunan Univ. Sci. Technol.: Nat. Sci.* **26**(3), 1–6 (2011).
19. Xie, W., Peng, Y., Wu, L. & Li, X. Numerical analysis on acoustic field characteristics of excavation roadway based on surface integration method. *J. China Coal Soc.* **36**(11), 1790–1794 (2011).
20. Yang, M. et al. Effect of variation of cross section dimensions on noise propagation in coal mine excavation roadway. *China Saf. Sci. J.* **34**(4), 77–86 (2024).
21. Zhai, C. et al. Noise propagation law of local ventilator straight roadway with different surface roughness. *Saf. Coal Mines.* **47**(8), 26–29 (2016).
22. Jing, G., Guo, S., Wang, Y. & Zhou, F. Simulated study of the noise field of fully mechanized mining face based on the finite element method and situational experiment. *J. Saf. Environ.* **19**(06), 1978–1983 (2019).
23. Yang, M. et al. Influence of roadway layout on sound field distribution in fully mechanized mining face system. *J. Saf. Environ.* **23**(10), 3666–3674 (2023).
24. Xie, L. et al. Comparison of acoustic attenuation characteristics of typical shape earplugs. *Tech. Acoust.* **37**(6), 4–5 (2018).
25. National Health Commission of the People's Republic of China. Design hygiene standards for industrial enterprises (GBZ 1-2024) (S). Beijing: China Standards Press, (2024).
26. Mao, D. X. & Hong, Z. H. Environmental noise control engineering. Beijing: Higher Education Press 93-95 (2012).
27. Shen, X. & Sun, H. Finite element method in engineering acoustics. *Acta Acustica.* **4**, 249–259 (1981).
28. Savioja, L. & Svensson, U. P. Overview of geometrical room acoustic modeling techniques. *J. Acoust. Soc. Am.* **138**(2), 708–730 (2015).
29. Feng, T. & Wang, J. Numerical methals and their application scope in acoustic field. *J. Beijing Technol. Bus. Univ.* **33**(1), 41–43 (2004).
30. Yang, L. N. & Shield, B. M. Development of a ray tracing computer model for the prediction of the sound field in long enclosures. *J. Sound & Vib.* **229**(1), 133–146 (2000).
31. Zhang, Z., Bai, Y., Guo, C. & Cheng, J. Noise propagation characteristics of tunnel construction by drilling and blasting method. *Tunn. Constr.* **40**(6), 821–826 (2020).
32. Ma, D. *Handbook of noise and vibration control engineering* (China Machine Press, 2002).
33. Sadeghi, S., Soltanmohammadlou, N. & Nasirzadeh, F. Applications of wireless sensor networks to improve occupational safety and health in underground mines. *J. Saf. Res.* **83**(8), 25 (2022).
34. Zheng, J., Li, L. & Daviault, M. Experimental study on the effectiveness of lubricants in reducing sidewall friction. *Int. J. Geomech.* **21**(5), 04021079 (2021).

Author contributions

Gaini Jia: Conceptualization, Formal analysis, Investigation, Methodology, Writing - original draft, Writing-review & editing; Ming Yang, Dongjie Jiang and Junjie Guo: Writing - Review & Editing, Funding acquisition and Supervision; Maomao Liu and Yunqi Tao: Methodology, Visualization, Writing-review & editing

Funding

This work was supported by the National Natural Science Foundation of China (Grant Nos. 52274186, 52274187) and the Henan Provincial Key Scientific and Technological Research Project (Grant No. 252102220013).

Declarations

Competing interests

The authors declare that they have no known competing financial interests or personal relationships that could have appeared to influence the work reported in this paper.

Additional information

Correspondence and requests for materials should be addressed to M.Y. or D.J.